

# Effect of Oxidation Behavior on the Mechanical and Thermal Properties of Plasma Sprayed Tungsten Coatings

Deyang Hu, Xuebin Zheng, Yaran Niu, Heng Ji, Fali Chong, and Junling Chen

(Submitted September 9, 2007; in revised form January 15, 2008)

Tungsten (W) coatings have been prepared via air (APS) and vacuum plasma spraying (VPS) technologies, respectively. The microstructures and chemical compositions of the coatings were comparatively studied; meanwhile, the mechanical and thermal properties were evaluated. The results obtained showed that oxide content in the VPS-W coating was apparently lower than that of the APS-W coating because of the different surrounding atmosphere, which influenced the mechanical and thermal properties of the coatings directly. Similar microstructures were observed for the VPS-W and the APS-W coating, but the VPS-W coating was much denser. The bonding strength of the VPS-W coating was much higher than that of the APS-W coating. Thermal conductivity of the VPS-W coating was 59.3 W/m · K at room temperature while the APS-W coating was 32.2 W/m · K. Thermal loading experiments of electron beam showed that the VPS-W coating could withstand the heat load of 10.75 MW/m<sup>2</sup>, while the APS-W coating formed serious cracks on its surface at the load of 7.5 MW/m<sup>2</sup>.

**Keywords** APS, bonding strength, thermal conductivity, thermal loading experiment, tungsten coating, VPS

## 1. Introduction

CFC, B<sub>4</sub>C, Be, W, Mo, V, and so forth have been studied as candidates for plasma facing materials (PFM) in fusion experiment devices (Ref 1-3). However, the low-Z materials such as Be and C are susceptible to erosion under plasma particles bombardment by physical sputtering, radiation-enhanced sublimation, and chemical sputtering processes (Ref 4). The erosion not only contaminates the plasma but also changes the properties of the plasma facing wall (Ref 5).

It has been demonstrated that W has many special advantages as PFM in recent research, such as: highest melting point of all metals, high energy threshold for physical sputtering, low deuterium etching, good thermal conductivity, high-temperature strength, and dimensional stability (Ref 6). The main drawbacks of W are the high ductile-to-brittle transition temperature (DBTT, about 400 °C) and difficulties in machining (Ref 7). So it is significant to use W coatings at plasma facing surfaces

instead of W bulk materials. The preparation and characterization of W coating have been actively studied. Several coating technologies have been applied to fabricate W coatings. Nakamura et al. (Ref 8) prepared W coating via chemical vapor deposition (CVD), and Deschka et al. (Ref 9) used physical vapor deposition (PVD). The high cost and thin thickness of the CVD-W coating limited the application of this method, while the main problems in the PVD-W coating were the low adhesion and high impurity content. Maier et al. (Ref 10) compared W film deposited by magnetron sputtering (MS) and by plasma arc (PA) deposition. It was reported that high compressive stress led to delamination when a MS-W film thickness was about 3 μm, and for the PA-W film it was not suitable for thick coatings as well. To achieve inexpensive, thick W coatings with good adhesion strength, Riccardi et al. (Ref 11) fabricated W coating through plasma spraying (PS) technology. Matějčíček et al. (Ref 12) exposed the PS-W coatings to high-temperature plasma in a small tokamak, and the coatings showed no erosion and minimal influence on plasma parameters. Boire-Lavigne et al. (Ref 13) investigated the thermal diffusivity using laser flash method and found that spraying atmosphere had a strong influence on the interfacial contact between lamellas and the thermal diffusivity of the PS-W coatings.

Plasma spray technology enables the preparation of a broad variety of coating materials, including high melting point materials. Plasma spray technology has become the favorite way to prepare W coating now, because of its ability to cover large surfaces with thick coatings and its relatively low cost. However, the intrinsic porosity and high impurity content decrease the mechanical and thermal properties of PS-W coating. Greuner et al. (Ref 14) thought that parallel layer structure and porosity of layer

**Deyang Hu, Xuebin Zheng, Yaran Niu, and Heng Ji**, Shanghai Institute of Ceramics, Chinese Academy of Sciences, 1295 Dingxi Road, Shanghai 200050, People's Republic of China; and **Fali Chong and Junling Chen**, Institute of Plasma Physics, Chinese Academy of Sciences, P.O. Box 1126, Hefei 230031, People's Republic of China. Contact e-mails: xbzheng@mail.sic.ac.cn and hudeyang9@mail.sic.ac.cn

reduced the thermal conductivity of the coatings ( $20 \text{ W/m} \cdot \text{K}$  at room temperature), while Kang (Ref 15) pointed out that tungsten oxide and porosity in the coating might have a significant influence on its electrical and thermal conductivity.

There have been some studies on the PS-W coating focused on the microstructures and thermal responses under high heat loads, but little research was carried out concerning the effects of oxidation behavior on the mechanical and thermal properties of the coatings. In this work, an effort was made to investigate the influence of oxygen impurity on the properties of PS-W coatings. Two kinds of coatings have been prepared via air plasma spray (APS) and vacuum plasma spraying (VPS) technologies, respectively. The influence of oxidation behavior on their microstructures, chemical compositions, microhardness, bonding strengths, and thermal conductivities were investigated. Thermal loading experiments were also carried out to evaluate the high heat flux properties of the coatings.

## 2. Experimental Procedure

Commercially available tungsten powder with a median size of  $42 \mu\text{m}$  in a weight mean (Fig. 1) was applied to prepare coatings via a plasma spray system (Sulzer Metco A-2000, Switzerland) equipped with a F4-MB torch for APS and a F4-VB torch for VPS, respectively. For both APS and VPS processing, argon and hydrogen were used as plasma forming gases, and the coatings were deposited onto copper (Cu) substrate under modified deposition

parameters (Table 1). Before deposition, the Cu substrate was grit blasted and the gradient layer comprising W and Cu was applied to improve the bonding strength of the coating. The gradient layer was stepped from 1:1, 1:2, to 1:3 at the weight ratio of Cu and W, the total thickness of which was about  $80 \mu\text{m}$ .

Microstructures of the coatings were characterized by an electron probe microscope analyzer (EPMA; JAX-8100, JEOL, Japan) and a transmission electron microscope (TEM; TEM-2100F, JEOL, Japan). Porosity was determined using OPTILABA and IMAGE (from the National Institute of Health (NIH), Springfield, VA) software and the cross-sectional SEM images of the coatings were used. X-ray energy dispersive spectrometry (EDS; TEM-2100F, JEOL, Japan) and Auger electron spectroscopy (AES; Microlab 310F with a dual-anode, VG Scientific, Great Britain) were applied to examine the chemical compositions and structures of the coatings. Polished specimens of W coatings were used in AES examination. The oxygen content in the coatings was detected by Nitrogen/Oxygen Determinator (TC600, Leco, USA).

**Table 1** Spraying parameters of APS and VPS

	VPS	APS
Plasma gas Ar, slpm	42	40
Plasma gas H <sub>2</sub> , slpm	10	10
Spray distance, mm	300	150
Chamber pressure, mbar	100	...
Powder carrier gas, Ar, slpm	3.0	4.0
Power, kW	39	36
Spray gun	F4-VB	F4-MB

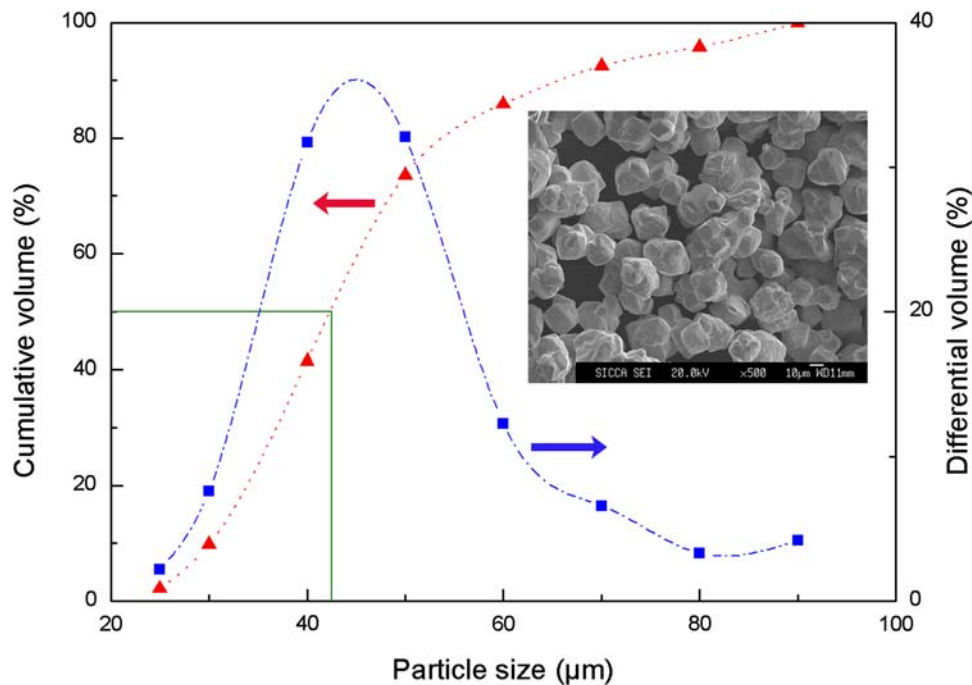


**Fig. 1** Particle size distribution of W feedstock and its SEM photograph

The bonding strengths of the coatings were evaluated according to ASTM C 633–79. The Vickers microhardness tests of the as-sprayed coatings were performed on polished surfaces (cross sections of the coatings) by a microhardness tester (HX-1000, SSOIF, China) with a 1.96 N normal load and a dwell time of 15 s. The reported values of microhardness of the coatings were the mean of 20 indentations. To avoid the effect of stress field, the distance between two indentations was kept greater than three times the indentation diagonal (Ref 16). Thermal conductivities of the coatings were measured on a physical property measurement system (PPMS; PPMS Model 6000 Quantum Design). The temperature ranged from 2 to 320 K with the infrared emissivity  $\varepsilon = 0.3$  (Ref 17).

Thermal loading experiments were carried out with active water cooling in an e-beam high heat flux (HHF) test facility. The coatings of 1 mm thickness including the gradient layer were sprayed on Cu substrates of an area of  $40 \times 30$  mm and a height of 25 mm. An electron beam with particle energy of 10 keV was used in the tests, and the water flow rate was  $1.8 \text{ m}^3/\text{h}$ . The loaded area was  $2 \text{ cm}^2$ , and the chamber pressure was  $2.3 \times 10^{-3}$  to  $3.2 \times 10^{-3}$  Pa. The heat load increased with a stepwise increase of  $1.25 \text{ MW}/\text{m}^2$ , and each step lasted for 100 s. The starting heat loads for the tests were  $2.5 \text{ MW}/\text{m}^2$ . The surface temperature variation of the coatings was measured by an infrared (IR) pyrometer, the wavelength of which was 0.85 to  $1.08 \text{ }\mu\text{m}$ . It had one color, and the measurable temperature range was from 500 to  $2000 \text{ }^\circ\text{C}$ .

### 3. Results and Discussion

#### 3.1 Microstructure and Chemical Composition

Figure 2 shows the surface morphologies of APS-W and VPS-W coatings. Well-molten particles were observed in both of the coatings; however, it was found that there were distinct microcracks on the surface of the APS-W coating (Fig. 2a). The fracture morphologies of W coatings are shown in Fig. 3. Lamellar structures characteristic of plasma sprayed coatings and columnar crystals were found in both coatings, and the grain boundary was clearly viewed in the VPS-W coating. Similar columnar crystal structure of W coating deposited on molybdenum substrate was reported in Du et al. (Ref 18). The microstructure showed that VPS-W coating had less porosity than that of APS-W coating. Two kinds of typical micropores were observed in the APS-W coating (Fig. 3a): one was spherical pores with a diameter about  $4 \text{ }\mu\text{m}$ , and the other was linear pores with an average length about  $6 \text{ }\mu\text{m}$ . Microcracks were also found in the APS-W coating, while no cracks and fewer micropores were discovered in the VPS-W coating (Fig. 3b). Porosity in the APS-W coating was 10.2%, while porosity was only 2.1% in the VPS-W coating determined by image analysis, and the sample photos used for porosity measurement are shown in Fig. 4.

The transverse sectional (perpendicular to the spraying direction) microstructure characteristics of W coatings are

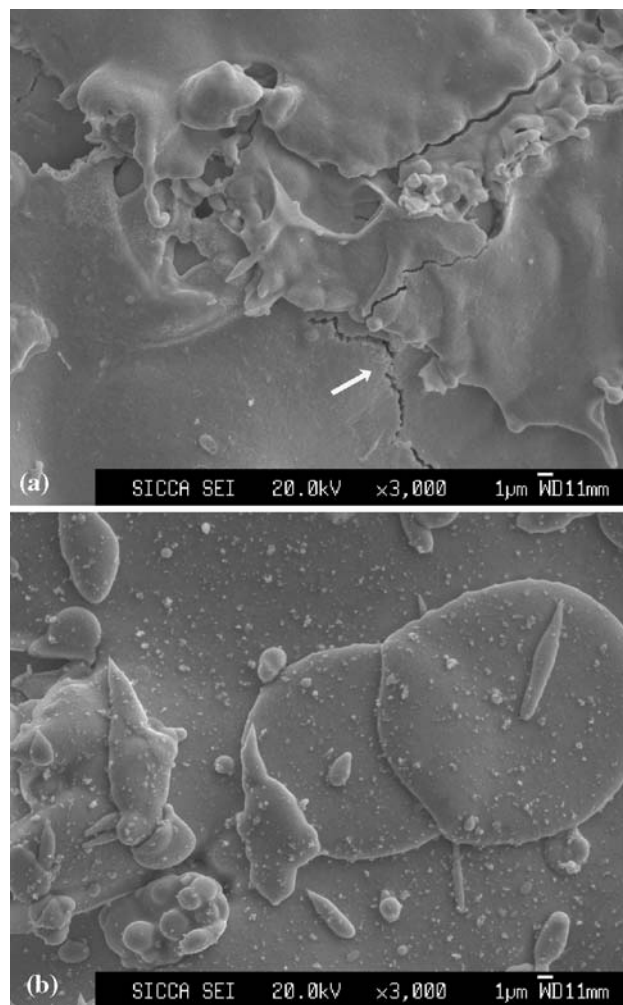


**Fig. 2** Surface morphologies of plasma sprayed W coatings: (a) APS-W and (b) VPS-W

presented in Fig. 5. It could be seen that both coatings were composed of W crystalline grains with different sizes and irregular shapes. The average grain size in the VPS-W coating was  $0.78 \text{ }\mu\text{m}$ , which was about twice that in the APS-W coating ( $0.34 \text{ }\mu\text{m}$ ). The difference in grain size was determined by the different cooling conditions during spray process. The VPS-W coating was deposited and cooled down in the chamber without air cooling during and after the fabrication process, but for the APS-W coatings there was an air-cooling system. Therefore, the substrate temperature was much higher than the APS-W coating, and the cooling rate was lower as well, which resulted in lower nucleation rate and larger grain size for the VPS-W coating. The diffraction spot of the VPS-W coating was circular, while that of the APS-W coating was arc ellipse in the electron diffraction patterns, which suggested that the crystallization in the APS-W coating was not as good as that in the VPS-W coating (Ref 19). EDS spectra of as-sprayed W coatings are also shown in Fig. 5. Oxygen peak was found in the APS-W coating, but not viewed in the VPS-W coating.



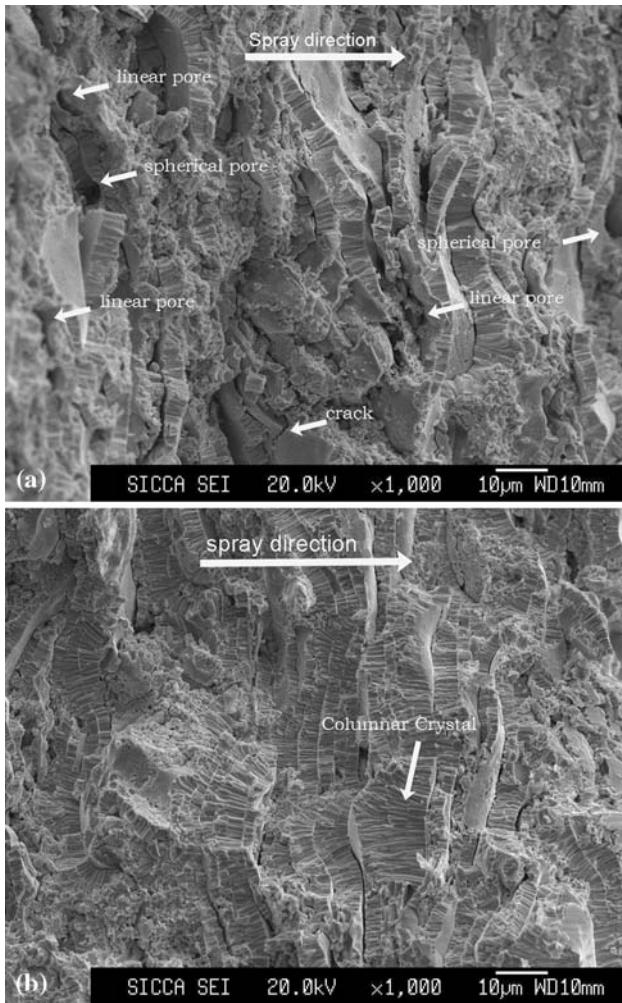
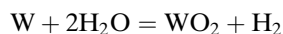


**Fig. 3** Fracture surface SEM images of plasma sprayed W coatings: (a) APS-W and (b) VPS-W

Generally, tungsten oxide is generated from the reaction between W and O<sub>2</sub> during the deposition of APS-W coating. Meanwhile, some researchers believed that the presence of H<sub>2</sub>O, which comes from the environment moisture and the reaction between H<sub>2</sub> and O<sub>2</sub>, also played an important role in the oxidation of tungsten. Hegetüs et al. (Ref 20) proposed tungsten oxide was produced at 740 °C:



Bigey et al. (Ref 21) believed that tungsten oxide changed—for example, WO<sub>2</sub>, WO<sub>3</sub>, WO<sub>2.9</sub>, WO<sub>2.72</sub>, and so forth—at different temperatures. The oxygen examination result obtained by Nitrogen/Oxygen Determinator showed that the oxygen content was about 0.21 wt.% in the APS-W coating and about 0.07 wt.% in the VPS-W coating. Unfortunately, no tungsten oxide phase was found in the XRD patterns because of the XRD detection limit (2 wt.%).

The AES spectra of the W coatings in different depths under the polished surface are presented in Fig. 6. It could

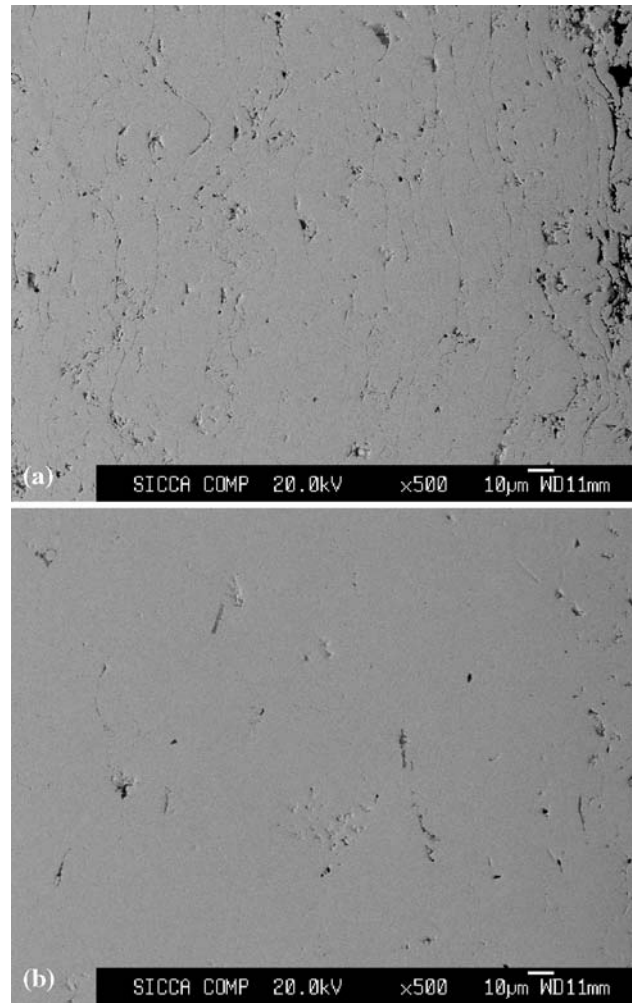


**Fig. 4** The example photos of W coating used for porosity measurement: (a) APS-W and (b) VPS-W

be seen that O peaks appeared on the outmost layers (depth=0 nm) of the both coatings. For the VPS-W coating, the height of O peak decreased with the increasing depth, and the O peak almost disappeared at a depth of 36 nm (Fig. 6b). However, it was found that oxygen peak presented apparently at all depths for the APS-W coating, which confirmed that oxide did exist in the coating (Fig. 6a). The oxygen on the surface of the VPS-W coating was supposed to be introduced from exposure to air after spraying or during the polishing process.

### 3.2 Mechanical Properties

The microhardness of the VPS-W coating was  $2.71 \pm 0.52$  GPa, which was 77% of bulk W (3.5 GPa), while the APS-W coating was  $2.44 \pm 0.46$  GPa which was 69% of W bulk material. The high value of microhardness of the VPS-W coating benefited from the lower porosity and fewer defects (Fig. 3) because of less oxidation. Polcar et al. (Ref 22) prepared tungsten oxide coatings with

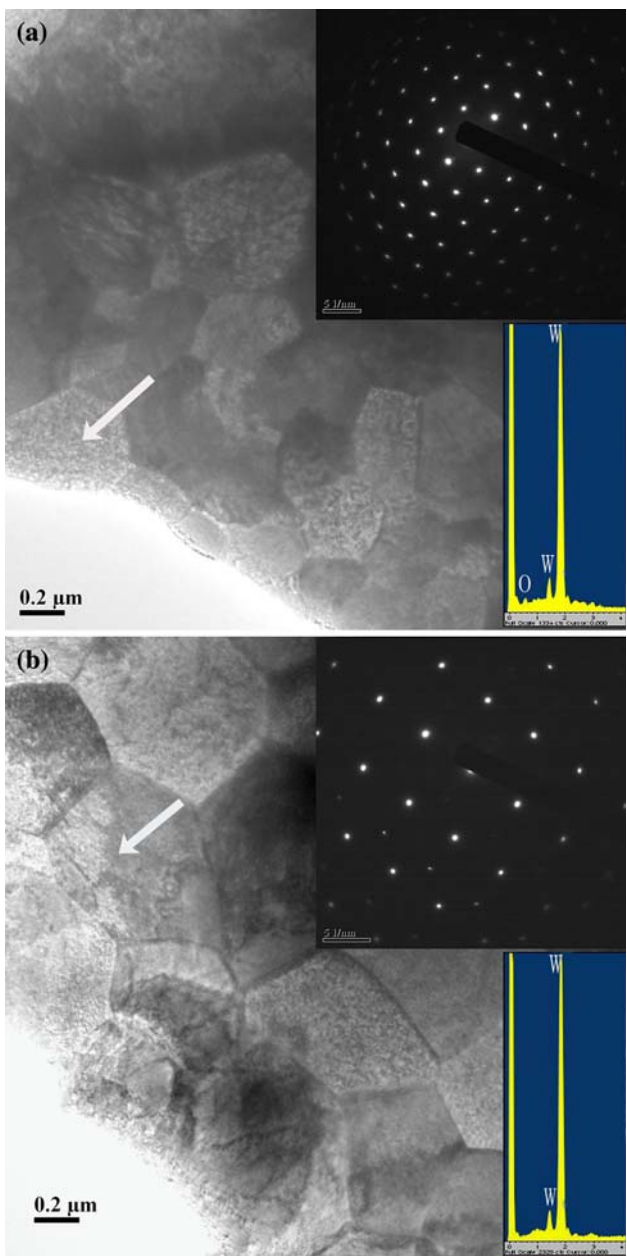


**Fig. 5** Transverse sectional TEM morphologies of plasma sprayed W coatings: (a) APS-W and (b) VPS-W

13 and 75 at.% oxygen content by direct current (dc) magnetron sputtering and found that the coating hardness decreased with increasing oxygen content from 25 to 7.7 GPa. It was thought that the oxidation affected the texture of the coating by introducing more pores and some other defects, which had an important influence on the microhardness (Ref 23).

The bonding strength tests of the coatings revealed that the bonding strength of the VPS coating was 44.8 MPa, which was about twice that of the APS coating (22.7 MPa) (Fig. 7). The good adhesion between the VPS-W coating and substrate were explained in terms of less oxidation

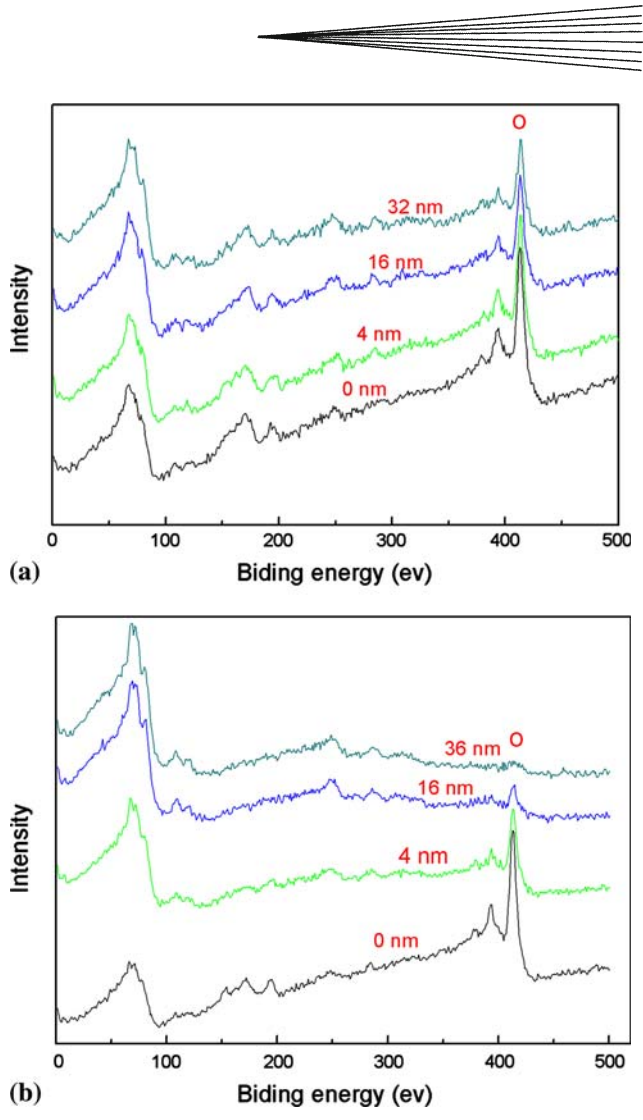


**Fig. 6** AES spectra of plasma sprayed W coatings: (a) APS-W and (b) VPS-W

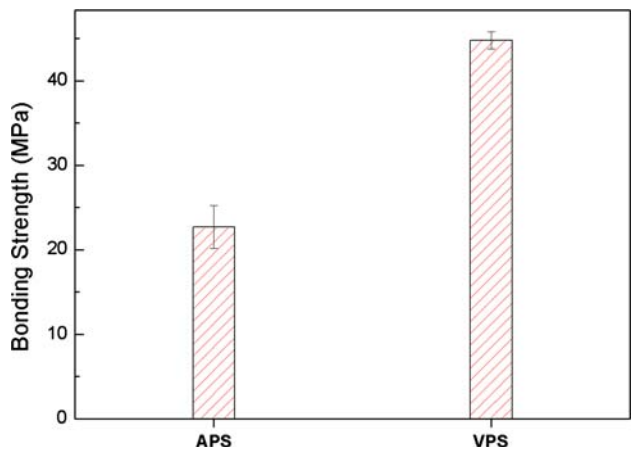


**Fig. 7** Bonding strength of plasma sprayed W coatings

and higher flight velocity of W particles during vacuum plasma spraying process (Ref 24). The bonding strength was influenced by the thermal and kinetic energy of the

particles; however, tungsten oxide has low boiling point ( $\text{WO}_3$  for example is  $1840^\circ\text{C}$ ), the evaporation of which during spraying reduced the particle energy (Ref 25). Then higher kinetic energy was allowed by higher flight velocity, and higher thermal energy was provided by less oxidation for the VPS-W coating. Parreira et al. (Ref 26) found that the adhesion of the sputtered tungsten oxide coating was much better for the low oxygen content than that for the high oxygen content. Different broken modes were found in the tensile test from the images of the fracture surfaces. The color of the APS-W coating fracture surface was taupe, the typical color of mixed Cu and W. Meanwhile, the VPS-W coating fracture surface was reddish, which was the same color of copper. The observation of the fracture surfaces revealed that during the bonding strength tests, the APS-W coating failed in the gradient layer, while the VPS-W coating ruptured at the boundary between coating and substrate. This revealed that the copper oxide and tungsten oxide in the Cu-W gradient layer of the APS-W coating greatly decreased the bonding strength. The higher mismatch stress was enhanced by the oxidation, and more porosity (Fig. 4a) in the APS-W coating might reduce the adhesion between coating and substrate (Ref 27, 28).

### 3.3 Thermal Conductivity

The variations of thermal conductivity versus temperature for the VPS-W and APS-W coatings are exhibited in Fig. 8. It was discovered that the thermal conductivity of the VPS-W coating was about  $59.3 \text{ W/m} \cdot \text{K}$  at room temperature, which was much higher than that of the APS-W coating ( $32.2 \text{ W/m} \cdot \text{K}$ ).

Thermal conductivity of plasma sprayed W coating depends strongly on the texture structure, defects, porosity, and oxide impurity, which are determined in the fabrication process. Castro et al. (Ref 29) demonstrated that the thermal conductivity of Be coating decreased with increasing porosity. Riccardi et al. (Ref 30) thought that the lamellar structure of the coating reduced its thermal

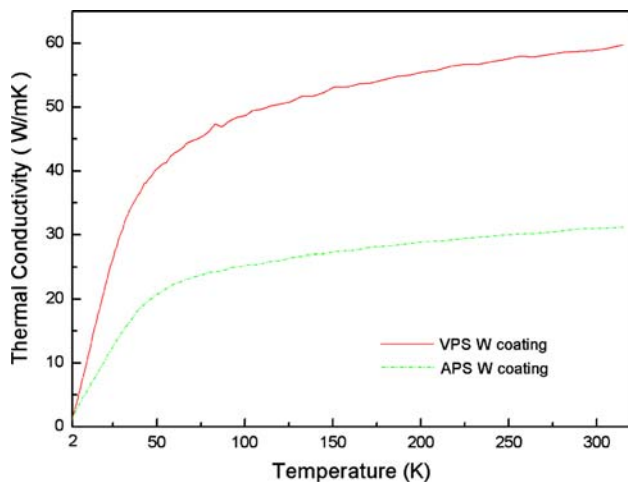


Fig. 8 Thermal conductivities of plasma sprayed W coatings

conductivity. It was supposed that the gaps between the parallel layers (Fig. 3a) and more grain boundaries in the APS-W coating limiting the electron mean free path by means of scattering also influenced the thermal conductivity of the coating. High oxygen content in the APS-W coating contributed to the reduced thermal transfer as well compared to VPS-W coating. Kang (Ref 15) showed evidence that tungsten oxide had some influence on the thermal diffusivity ( $\alpha$ ). Generally, the thermal conductivity ( $\kappa$ ) is determined by:  $\kappa = \rho_s \cdot C_p \cdot \alpha$ , where  $C_p$  is the specific heat and  $\rho_s$  is the sintered density. Lower thermal diffusivity and higher porosity reduced the thermal conducting ability of APS-W coating significantly.

### 3.4 Thermal Loading Test

Surface temperature evolutions measured by an IR camera during thermal loading tests are given in Fig. 9. The surface temperature of the APS-W coating increased quickly with the flux rising from the flux of  $2.5 \text{ MW/m}^2$ . It was not sensitive for the IR pyrometer below  $600^\circ\text{C}$ , and the temperature of the VPS-W coating was below that when the flux was less than  $6.25 \text{ MW/m}^2$ . Therefore, the temperature curve of the VPS-W coating was drawn from  $6.25 \text{ MW/m}^2$ . The surface temperature of the APS-W coating was  $1290^\circ\text{C}$  at  $7.5 \text{ MW/m}^2$ , while it was only  $1160^\circ\text{C}$  for VPS-W coating at  $10.75 \text{ MW/m}^2$ . The higher thermal conductivity of VPS-W coating was helpful to transfer the heat to the cooling substrate and decreased the surface temperature. Surface morphologies of the W coatings after thermal loading tests are shown in Fig. 10. Recrystallization textures were found in both coatings. Similar recrystallization phenomenon of plasma sprayed W coating was found by Liu et al. using annealing and cyclic heat load experiments (Ref 31). It was reported by Tamura et al. (Ref 32) that the recrystallization influenced the mechanical properties such as the embrittlement in the cyclic heat load tests (Tamura et al.). No distinct micro-cracks were found in the VPS-W coating after the thermal load of  $10.75 \text{ MW/m}^2$ , as shown in Fig. 10(b). However,

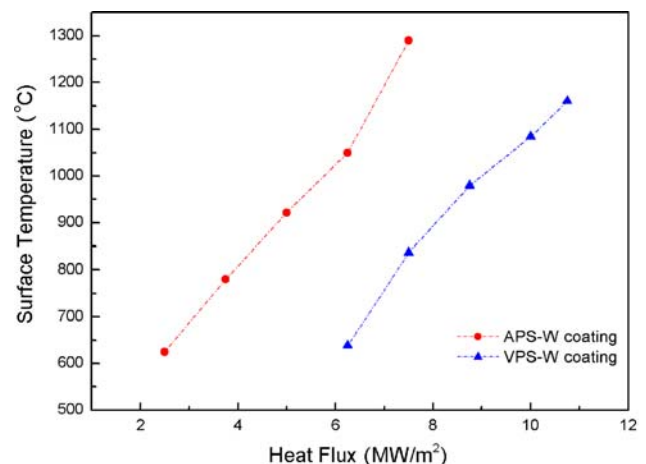
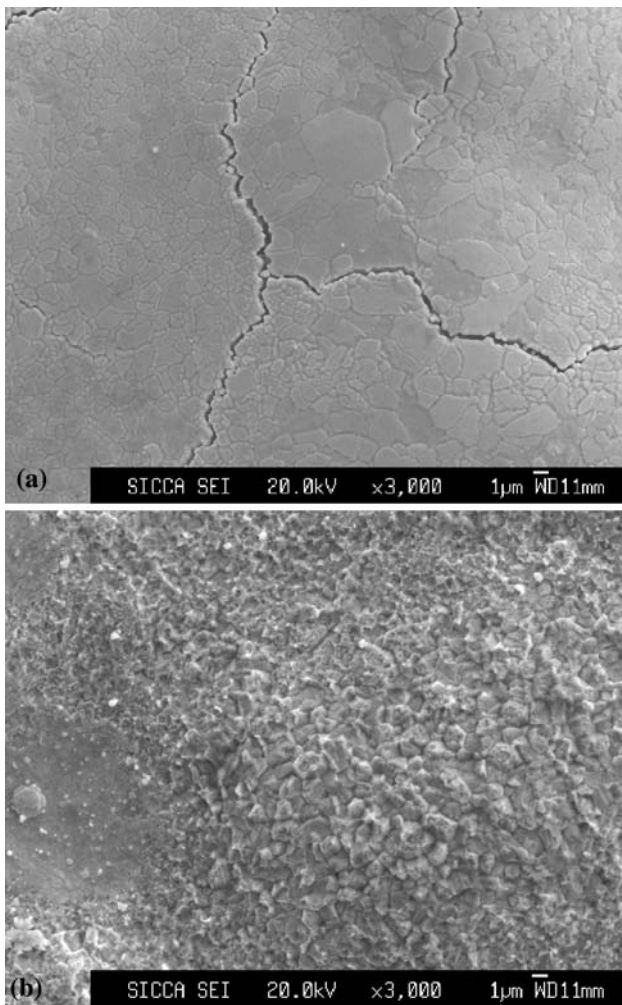
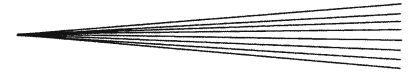


Fig. 9 Surface temperatures of plasma sprayed W coatings during thermal loading tests





**Fig. 10** Surface morphologies of W coatings after thermal load tests: (a) APS-W and (b) VPS-W

obvious microcracks were found in the APS-W coating (Fig. 10a). Tokunaga et al. (Ref 33, 34) believed that crack creation was attributed to the local thermal stress. During the thermal loading tests, high heat flux led to the reinforcing of thermal stress on the surface. Because of the low value of the thermal conductivity of APS-W coating, the heat on the surface could not be relaxed quickly and then the surface coating became more brittle during cooling, which resulted in the creation of cracks. Additionally, the oxide impurity, which had different thermal expansion behaviors (the CTE value of W and  $\text{WO}_3$  are  $4.5 \times 10^{-6} \text{ K}^{-1}$  and  $16.4 \times 10^{-6} \text{ K}^{-1}$ , respectively, Ref 35) augmented the stress when the temperature increased.

#### 4. Conclusions

Tungsten coatings have been deposited on the copper substrate via air and vacuum plasma spraying technologies, respectively. Higher oxygen impurity (0.21 wt.%),

more microcracks, and higher porosity were found in the APS-W coating than in the VPS-W coating. Spherical pores and linear pores were observed in the APS-W coating, which decreased the microhardness. Different broken modes in the bonding strength tests between APS-W and VPS-W coatings suggested that oxide impurity reduced the bonding strength significantly. Thermal conductivity of the VPS-W coating was  $59.3 \text{ W/m} \cdot \text{K}$  at room temperature, while the APS-W coating was  $32.2 \text{ W/m} \cdot \text{K}$ . Oxide impurity, lamellar structure, and intrinsic porosity of coating were responsible for the low thermal conductivity of the APS-W coating. Thermal loading experiments of electron beam showed that the VPS-W coating could withstand the heat flux of  $10.75 \text{ MW/m}^2$ , while the APS-W coating caused microcracks to propagate and extend on its surface at  $7.5 \text{ MW/m}^2$  load. It was found that oxidation behavior strongly affected the mechanical and thermal properties of PS-W coatings; therefore, it becomes important to further reduce the oxygen impurity in future studies.

#### References

1. B. Vastra, B. Schedler, M. Merola, F. Jacquinet, A. Cottin, D. Cauvin, M. Febvre, and Y. Leblanc, Manufacturing of Prototype Components for the ITER Divertor Baffle, *Fusion Eng. Des.*, 2003, **66-68**, p 341-346
2. N. Yoshida, Review of Recent Works in Development and Evaluation of High-Z Plasma Facing Materials, *J. Nucl. Mater.*, 1999, **266-269**, p 197-206
3. H. Maier, J. Luthin, M. Balden, J. Linke, F. Koch, and H. Bolt, Properties of Tungsten Coatings Deposited onto Fine Grain Graphite by Different Methods, *Surf. Coat. Technol.*, 2001, **142-144**, p 733-737
4. A. Cambe, E. Gauthier, J.M. Layet, and S. Bentivegna, Development of Tungsten Coating for Fusion Applications, *Fusion Eng. Des.*, 2001, **56-57**, p 331-336
5. S. Tamura, K. Tokunaga, and N. Yoshida, Damage Process of Resolidified Part on CVD-W Coated Molybdenum under High Heat Load, *J. Nucl. Mater.*, 2003, **313-316**, p 250-254
6. J. Matějček, P. Chráska, and J. Linke, Thermal Spray Coating for Fusion Applications—Review, *J. Therm. Spray Technol.*, 2007, **16**(1), p 64-83
7. T. Hirai, A. Kreter, J. Malzbender, T. Ohgo, V. Philipps, G. Pintsuk, A. Pospieszczyk, Y. Sakaw, G. Sergienko, T. Tanabe, Y. Ueda, and M. Wada, Critical Heat Flux Loading Experiments on CVD-W Coating in the TEXTOR Tokamak, *Fusion Eng. Des.*, 2006, **81**, p 175-180
8. K. Nakamura, S. Suzuki, T. Tanabe, M. Dairaku, K. Yokoyama, and M. Akiba, Disruption Erosions of Various Kinds of Tungsten, *Fusion Eng. Des.*, 1998, **39-40**, p 295-301
9. S. Deschka, C. Garcia-Rosales, W. Hohenauer, R. Duwe, E. Gauthier, J. Linke, M. Lochter, W. Mallener, L. Plöchl, P. Rödhammer, and A. Salito, Manufacturing and High Heat Flux Loading of Tungsten Coatings on Fine Grain Graphite for the ASDEX-upgrade Divertor, *J. Nucl. Mater.*, 1996, **233-237**, p 645-649
10. H. Maier, J. Luthin, M. Balden, S. Lindig, J. Linke, V. Rohde, H. Bolt, and ASDEX Upgrade Team, Development of Tungsten Coated First Wall and High Heat Flux Components for Application in ASDEX Upgrade, *J. Nucl. Mater.*, 2002, **307-311**, p 116-120
11. B. Riccardi, A. Pizzuto, A. Orsini, S. Libera, E. Visca, L. Bertamini, F. Casadei, E. Severini, R. Montanari, R. Vesprini, P. Varone, G. Filacchioni, and N. Litunovsky, Tungsten Thick Coatings for Plasma Facing Components, *Proc. 18th Symp. Fusion Technology*, B. Beaumont, P. Libeyre, B. de Gentile, and G. Tonon, Eds. (Marseille, France, CEA), 1998, p 223-226

12. J. Matějček, Y. Koza, and V. Weinzettl, Plasma Sprayed Tungsten-Based Coatings and their Performance under Fusion Relevant Conditions, *Fusion Eng. Des.*, 2005, **75-79**, p 395-399
13. S. Boire-Lavigne, C. Moreau, and R.G. Saint-Jacques, The Relationship Between the Microstructure and Thermal Diffusivity of Plasma-sprayed Tungsten Coatings, *J. Therm. Spray Technol.*, 1995, **4**(3), p 261-267
14. H. Greuner, H. Bolt, B. Böswirth, S. Lindig, W. Kühnlein, T. Huber, K. Sato, and S. Suzuki, Vacuum Plasma-Sprayed Tungsten on EUROFER and 316L: Results of Characterisation and Thermal Loading Tests, *Fusion Eng. Des.*, 2005, **75-79**, p 333-338
15. H.-K. Kang, Thermal Properties of Plasma-Sprayed Tungsten Deposits, *J. Nucl. Mater.*, 2004, **335**, p 1-4
16. S.H. Leigh, C.K. Lin, and C.C. Berndt, Elastic Response of Thermal Spray Deposits under Indentation Tests, *J. Am. Ceram. Soc.*, 1997, **80**(8), p 2093-2099
17. PPMS-Hardware&Options Manuals, Quantum Design Co. Ltd., 2003, p 1-7
18. J. Du, Z. Li, G. Liu, H. Zhou, and C. Huang, Surface Characterization of CVD Tungsten Coating on Molybdenum Substrate, *Surf. Coat. Technol.*, 2005, **198**, p 169-172
19. P. Wang, X. Li, C. Lu, T. Chen, G. Chen, S. Zhuo, G. Tao, H. Gu, and L. Yu, Chemical and Structural Characterization for Advanced Inorganic Materials, 1st ed., Higher Education Press, Beijing, 2006, p 315-323 (in Chinese)
20. É. Hegetűs, J. Neugebauer, and M. Mészáros, Apparent Reversibility of the  $\beta$ -w  $\rightarrow$   $\alpha$ -w Transformation, *Int. J. Refract. Met. Hard Mater.*, 1998, **16**, p 31-35
21. C. Bigey, L. Hilaire, and G. Maire, Catalysis on Pd/WO<sub>3</sub> and Pd/WO<sub>2</sub>: Effect of the Modifications of the Surface States Due to Redox Treatments on the Skeletal Rearrangement of Hydrocarbons, *J. Catal.*, 1999, **184**, p 406-420
22. T. Polar, N.M.G. Parreira, and A. Cavaleiro, Tungsten Oxide with Different Oxygen Contents: Sliding Properties, *Vacuum*, 2007, **81**(11-12), p 1426-1429
23. C. Huang, X. Zhou, and C. Ding, Investigation of the Thermo-mechanical Properties of a Plasma-Sprayed Nanostructured Zirconia Coating, *J. Eur. Ceram. Soc.*, 2003, **23**(9), p 1449-1455
24. P. Zhang, Thermal Spray Materials, 1st ed., National Defense Industry Press, Beijing, 2006, p 8-10 (in Chinese)
25. J. Matějček, K. Neufuss, D. Kolman, O. Chumak, and V. Brožek, Development and Properties of Tungsten-based Coatings Sprayed by WSP, *Proc. International Thermal Spray Conference* (Basel, Switzerland), 2005, p 634-640
26. N. Parreira, N. Carvalho, and A. Cavaleiro, Synthesis, Structural and Mechanical Characterization of Sputtered Tungsten Oxide Coatings, *Thin Solid Films*, 2006, **510**(1-2), p 191-196
27. X.L. Zheng, S.R. Qiao, and X.P. Qin, Material Mechanical Properties, 2nd ed., Northwestern Polytechnical University Press, Xi'an, China, 2000, p 50, 54-56 (in Chinese)
28. A. Kucuk, C.C. Berndt, U. Senturk, and R.S. Lima, Influence of Plasma Spray Parameters on Mechanical Properties of Yttria Stabilized Zirconia Coatings. II: Acoustic Emission Response, *Mater. Sci. Eng. A*, 2000, **284**(1-2), p 41-50
29. R.G. Castro, A.H. Barlett, K.J. Hollis, and R.D. Fields, The Effect of Substrate Temperature on the Thermal Diffusivity and Bonding Characteristics of Plasma Sprayed Beryllium, *Fusion Eng. Des.*, 1997, **37**, p 243-252
30. B. Riccardi, R. Montanari, M. Casadei, G. Costanza, G. Filacchioni, and A. Moriani, Optimisation and Characterisation of Tungsten Thick Coatings on Copper Based Alloy Substrates, *J. Nucl. Mater.*, 2006, **352**, p 29-35
31. X. Liu, L. Yang, S. Tamura, K. Tokunaga, N. Yoshida, N. Noda, and Z. Xu, Thermal Response of Plasma Sprayed Tungsten Coating to High Heat Flux, *Fusion Eng. Des.*, 2004, **70**, p 341-349
32. S. Tamura, K. Tokunaga, N. Yoshida, M. Taniguchi, K. Ezato, K. Sato, S. Suzuki, M. Akiba, Y. Tsunekawa, and M. Okumiya, Damage Process of High Purity Tungsten Coatings by Hydrogen Beam Heat Loads, *J. Nucl. Mater.*, 2005, **337-339**, p 1043-1047
33. K. Tokunaga, N. Yoshida, N. Noda, T. Sogabe, and T. Kato, High Heat Load Properties of Tungsten Coated Carbon Materials, *J. Nucl. Mater.*, 1998, **258-263**, p 998-1004
34. K. Tokunaga, N. Yoshida, N. Noda, Y. Kubota, S. Inagaki, R. Sakamoto, T. Sogabe, and L. Plöchl, Behavior of Plasma-Sprayed Tungsten Coatings on CFC and Graphite under High Heat Load, *J. Nucl. Mater.*, 1999, **266-269**, p 1224-1229
35. Y.S. Touloukian, R.K. Kirby, R.E. Taylor, and T.Y.R. Lee, Thermophysical Properties of Matter, Vol. 13, Thermal Expansion Nonmetallic Solids. IFI/Plenum Press, New York, 1975, p 405